Tuning the Band Gap of Graphene Nanoribbons Synthesized from Molecular Precursors

Yen-Chia Chen,[†,‡,∥] Dimas G. de Oteyza,[†,§,∥] Zahra Pedramrazi,[†] Chen Chen,[⊥] Felix R. Fischer,[‡,⊥,*] and Michael F. Crommie[†,‡,*]

[†]Department of Physics, University of California at Berkeley, Berkeley, California 94720, United States, [‡]Materials Sciences Division, Lawrence Berkeley National Laboratory, Berkeley, California 94720, United States, [§]Centro de Física de Materiales CSIC/UPV-EHU-Materials Physics Center, San Sebastián, E-20018, Spain, and [⊥]Department of Chemistry, University of California at Berkeley, Berkeley, California 94720, United States. [∥]Y.-C. Chen and D. G. de Oteyza contributed equally.

ABSTRACT A prerequisite for future graphene nanoribbon (GNR) applications is the ability to fine-tune the electronic band gap of GNRs. Such control requires the development of fabrication tools capable of precisely controlling width and edge geometry of GNRs at the atomic scale. Here we report a technique for modifying GNR band gaps *via* covalent self-assembly of a new species of molecular precursors that yields $n = 13$ armchair GNRs, a wider GNR than those previously synthesized using bottom-up molecular techniques. Scanning tunneling microscopy and spectroscopy reveal that these $n = 13$ armchair GNRs have a band gap of 1.4 eV, 1.2 eV smaller than the gap determined previously for $n = 7$ armchair GNRs. Furthermore, we observe a localized electronic state near the end of $n = 13$ armchair GNRs that is associated with hydrogen-terminated sp^2-hybridized carbon atoms at the zigzag termini.

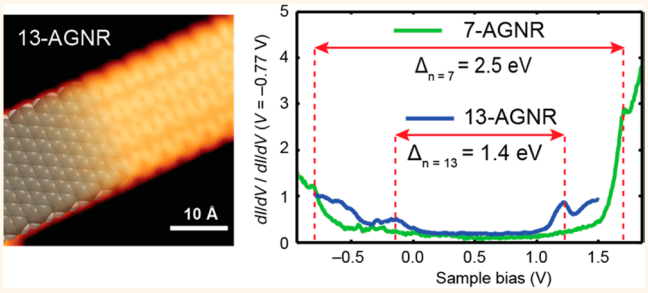

KEYWORDS: graphene nanoribbon · scanning tunneling microscopy and spectroscopy · molecular precursors · bottom-up synthesis · energy gaps

Graphene nanoribbons (GNRs) are two-dimensional strips of graphene featuring high aspect ratios and widths at the nanometer scale. Unique electronic and magnetic properties emerge from the structural boundary conditions imposed by the width, crystallographic symmetry, and edge structure of GNRs. The ability to control these GNR structural parameters with atomic precision is essential for tuning GNR properties between predicted behaviors such as correlated low-dimensional magnetism (*i.e.*, for zigzag GNRs (ZGNRs))[1−6] and strongly gapped semiconductor behavior (*i.e.*, for armchair GNRs (AGNRs)).[7−10] AGNRs, in particular, have emerged as a promising candidate for introducing device-relevant energy gaps—predicted to be inversely proportional to GNR width—into graphene.[7−10] While numerous top-down approaches have been used to produce GNRs,[11−17] these methods provide only limited control over the precise dimension and symmetry of the resulting GNRs. Recent advancements in the bottom-up synthesis of GNRs using molecular precursors provide a means for potentially overcoming these limitations.[18] This strategy has been used to synthesize atomically precise 7-AGNRs (the integer refers to the number of carbon dimer lines across the width of a GNR) from 10,10′-dibromo-9,9′-bianthracene (DBBA) building blocks.[18] Scanning tunneling microscopy (STM) and spectroscopy (STS) performed on 7-AGNRs have revealed an intrinsic band gap greater than 2.3 eV.[19,20] A shift in conduction band edge has also recently been observed for 7-AGNRs that undergo uncontrollable fusion to form wider ribbons.[21] Controlling the GNR structure by the appropriate selection of molecular precursors, however, remains a challenging task, as evidenced by the fact that no GNRs featuring widths greater than $n = 7$ have yet been synthesized in a controllable fashion using this technique.

* Address correspondence to ffischer@berkeley.edu, crommie@berkeley.edu.

Received for review April 18, 2013 and accepted June 9, 2013.

Published online June 09, 2013
10.1021/nn401948e

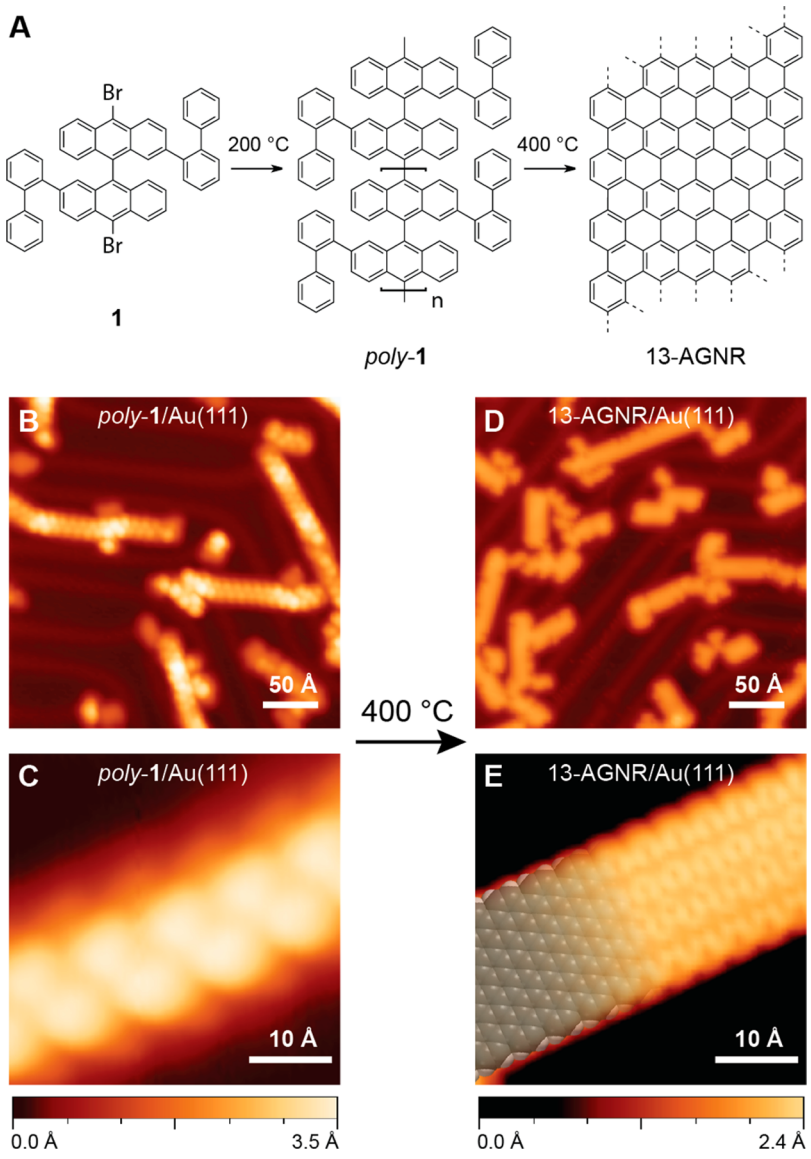

Figure 1. Synthesis of 13-AGNRs. (A) Schematic representation of the synthesis of 13-AGNRs from molecular building block 1. The precursor molecules 1 colligate to form polymers (poly-1) following the homolytic cleavage of the labile C−Br bonds at 200 °C on Au(111). At 400 °C a cyclization/dehydrogenation sequence converts the polymers to 13-AGNRs. (B) STM image of the polymer (poly-1) formed after the deposition of 1 onto a Au(111) surface held at 200 °C (V_s = 0.50 V, I_t = 3 pA). (C) High-resolution STM image of the polymer poly-1. The polymers are nonplanar with an apparent height of 3.5 Å (V_s = −0.30 V, I_t = 33 pA). (D) STM image of 13-AGNRs formed after annealing poly-1 at 400 °C (V_s = 0.50 V, I_t =12 pA). (E) Close-up STM image of a 13-AGNR (V_s = −0.70 V, I_t = 7.02 nA; a higher tunneling current was used here to obtain higher spatial resolution). A structural model of a 13-AGNR has been overlaid onto the STM image. Poly-1 tends to align with the Au(111) herringbone reconstruction, while 13-AGNRs do not exhibit a preferred orientation.

Here we report the synthesis and characterization of atomically precise n = 13 AGNRs fabricated using a radical step-growth polymerization of a newly developed small-molecule building block on Au(111) in ultrahigh vacuum (UHV). We have performed local electronic characterization of these new, wider GNRs using scanning tunneling microscopy and spectroscopy. The 13-AGNRs feature atomically smooth hydrogen-terminated armchair edges and 13 carbon dimer lines across their width. STS reveals the energy gap of these new GNRs to be 1.4 ± 0.1 eV, 1.2 eV smaller than the energy gap determined for narrower 7-AGNRs. We have also observed localized states at the ends of 13-AGNRs that extend up to 30 Å into the ribbons. These "end states" are associated with the zigzag structure of the 13-AGNR short edge (*i.e.*, the edge that terminates 13-AGNRs at their ends).

RESULTS AND DISCUSSION

In order to precisely control and expand the width of bottom-up-fabricated AGNRs we developed a small-molecule building block (**1**) derived from DBBA (see **1** in Figure 1A). 2,2′-Di((1,1′-biphenyl)-2-yl)-10,10′-dibromo-9,9′-bianthracene (**1**) was obtained through a Suzuki

cross-coupling reaction of 2,2′-dibromo-9,9′-bianthracene[22] (**2**) with (1,1′-biphenyl)-2-boronic acid followed by a selective bromination of the bianthracene core (see Scheme S1). The 13-AGNR building block **1** was subsequently sublimed under UHV onto a Au(111) surface maintained at 200 °C. Thermally induced homolytic cleavage of the labile C−Br bonds then generated sp^2 carbon-centered diradical intermediates,[23] which diffused on the surface and recombined with other diradicals in a step-growth polymerization to form linear chains of poly-**1** (Figure 1A). Annealing these AGNR precursors at 400 °C induced a stepwise cyclization/dehydrogenation sequence that yields fully conjugated 13-AGNRs (Figure 1A). A home-built low-temperature (T = 7 K) STM was used to characterize the polymer precursors poly-**1** (by cooling the sample from T = 200 °C to 7 K) as well as the fully cyclized 13-AGNRs (by cooling the sample from T = 400 °C to 7 K). STM spectroscopy was performed by measuring the differential conductance (dI/dV) of the STM tunnel junction.

Figure 1B shows an STM image of a representative sample of linear polymer chains formed from building block **1** after being deposited onto the Au(111) surface at 200 °C and subsequently cooled for imaging. The close-up image of the polymer chain in Figure 1C clearly exhibits a corrugated pattern along the backbone of the polymer chain. The maxima in this image alternate between the two opposite edges of the polymer chain. The apparent height of the polymer chains is 3.5 ± 0.3 Å, and the period of the corrugation is 9.5 ± 0.1 Å. The bright contrast along the center of the chain is consistent with protrusions expected to arise from the poly-anthracene subunits,[18] while contrast arising from the biphenyl groups lining the edges of the polymer is more diffuse. The significant deviation from planarity in the polymer is attributed to steric hindrance between hydrogen atoms in the *peri*-positions along the poly-anthracene backbone and has also been observed for polymer chains grown from DBBA.[18]

Figure 1D shows an STM image of the surface after annealing samples of poly-**1** at 400 °C for 5 min to complete the cyclization/dehydrogenation sequence. The di(biphenyl)-bianthracene subunits have fused into a fully conjugated linear nanoribbon (Figure 1D) featuring a width of 19 ± 2 Å and an apparent height of 2.1 ± 0.1 Å (significantly lower than the height of the polymer chains prior to cyclization/dehydrogenation). The close-up topographic image in Figure 1E confirms the atomically precise molecular structure of the resulting 13-AGNRs. These nanoribbons feature atomically smooth hydrogen-terminated armchair edges along the entire length of the ribbon and are composed of 13 dimer lines of carbon atoms at the widest point.

The local electronic structure of 13-AGNRs was characterized by performing STS measurements on

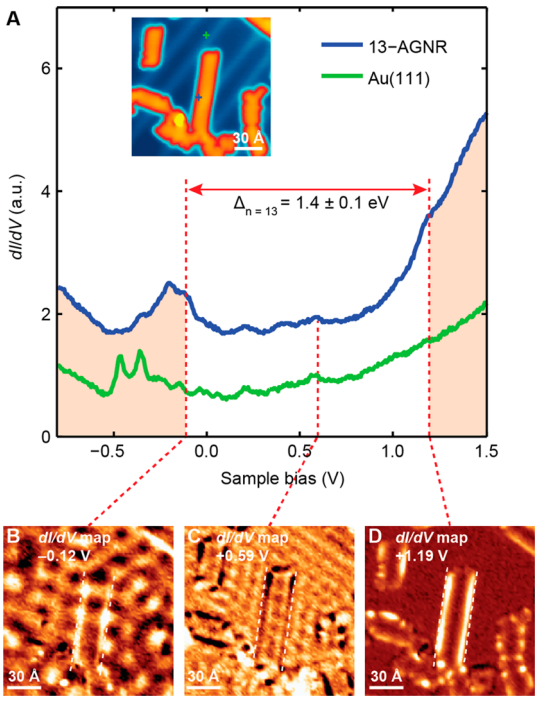

Figure 2. STM dI/dV spectroscopic measurement of 13-AGNR energy gap. (A) dI/dV spectra recorded on a 13-AGNR (blue line) and on bare Au(111) (green line). The 13-AGNR spectrum is offset vertically by 1 au for clarity (open-feedback parameters: V_s = 1.00 V, I_t = 35 pA; modulation voltage V_{rms} = 10 mV). Crosses in inset topographic image indicate the positions where spectra were recorded (inset V_s = 1.00 V, I_t = 35 pA). (B−D) dI/dV maps of 13-AGNR taken at (B) valence band edge (V_s = −0.12 V, I_t = 35 pA), (C) in the gap (V_s = 0.59 V, I_t = 35 pA), and (D) at the conduction band edge (V_s = 1.19 V, I_t = 35 pA). Dashed lines indicate the outer edges of the 13-AGNR. Band edge states have higher intensity near the edges of the GNR, while the GNR appears relatively featureless for energies within the gap.

15 different nanoribbons of varying lengths (from 3 nm up to 11 nm). A characteristic dI/dV spectrum of a 13-AGNR is shown in Figure 2A (blue line). The tunneling conductance (dI/dV) reflects the energy-dependent local density of states (LDOS) at the position beneath the STM tip. A spectrum recorded directly on the bare Au(111) substrate with the same STM tip serves as a background reference (green line). In the empty states (V > 0) the 13-AGNR dI/dV is featureless (other than simply reflecting the Au(111) and tip DOS) until a prominent shoulder rises that is centered at 1.19 eV above the Fermi energy (E_F). The magnitude of this shoulder varies from position to position on the GNR (and can also vary with different STM tips), and this feature often presents as a prominent peak rather than a shoulder (see Supporting Information), but its energy remains constant near the average value of 1.21 ± 0.06 V for all GNRs measured. We identify this feature as the 13-AGNR conduction band edge. Other empty state peaks in the 13-AGNR spectra are often observed at higher voltages (such as at ∼1.6 V), with their amplitudes also dependent on location within the GNR and the condition of the STM tip (see Supporting Information).

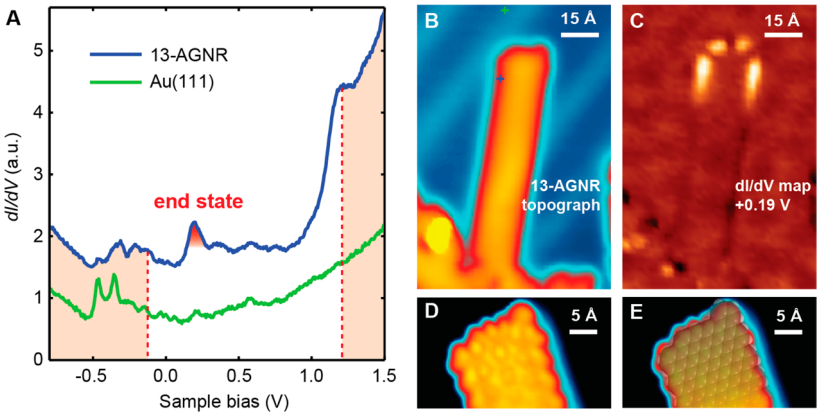

Figure 3. Localized end state of a 13-AGNR. (A) STM d*I*/d*V* spectra taken near the end of the same 13-AGNR shown in Figure 2 (blue line) and on bare Au(111) (green line) (open-feedback parameters: V_s = 1.00 V, I_t = 35 pA; modulation voltage V_{rms} = 10 mV). The GNR spectrum is offset vertically by 1 au for clarity. The spectra were recorded at the positions indicated by color-coded crosses in (B). The 13-AGNR spectrum exhibits an end-state resonance at +0.19 eV (shaded red). (B) STM topographic image of a 13-AGNR showing a nonreconstructed hydrogen-terminated end (V_s = 1.00 V, I_t = 35 pA). (C) d*I*/d*V* map at +0.19 V of the 13-AGNR in (B) shows that the end-state resonance is localized near the short edge of the GNR and extends only 30 Å along the GNR axis (open-feedback parameters: V_s = 1.00 V, I_t = 35 pA; modulation voltage V_{rms} = 10 mV). (D) Close-up STM image of the end of a different 13-AGNR (V_s = −0.05 V, I_t = 2.01 nA). (E) Structural model of the nonreconstructed end of a 13-AGNR overlaid onto the STM image shown in (D).

In the filled state part of the 13-AGNR d*I*/d*V* spectrum ($V < 0$) a broad resonance centered at ∼−0.2 V is the first prominent feature. This resonance also varies in magnitude for different positions on the GNR and with different tips, but the −0.2 V resonance is present on all 15 GNRs that we examined. Upon closer inspection, we observe that this resonance is composed of two energy-split resonances with the average energy splitting being 0.11 ± 0.04 eV (found *via* Lorentzian peak fitting; see Supporting Information, Figure S4). The filled-state resonance closest to E_F is always found centered near the average value −0.15 ± 0.04 V, and we identify this feature as the 13-AGNR valence band edge. Other GNR resonances in the filled states (with amplitudes depending on position and STM tip) are often seen at even lower energies (such as at ∼−0.6 V; see Supporting Information).

In summary, an average over all of our 13-AGNR spectra yields a conduction band edge at 1.21 ± 0.06 V and a valence band edge at −0.15 ± 0.04 V, thus leading to an average band gap for 13-AGNRs on Au(111) of Δ = 1.4 ± 0.1 eV. Narrower 7-AGNRs, by comparison, have an energy gap of Δ ≈ 2.6 eV using similar measurement criteria[19,20,24] (we have also measured an energy gap of Δ = 2.5 ± 0.1 eV for 7-AGNRs using the same instrument and characterization techniques that we used here for 13-AGNRs; see Supporting Information for further discussion of energy gap analysis).

To gain insight into the spatial distribution of the electronic structure of 13-AGNRs, we performed constant-bias d*I*/d*V* mapping (Figure 2B−D) of 13-AGNRs at different sample biases. Figures 2B and D show d*I*/d*V* maps at sample biases corresponding to the valence and conduction band edges, respectively. The bright intensity along the two longitudinal edges of the ribbon indicates a higher LDOS with respect to the gold surface at these energies (at some biases the surrounding gold surface shows oscillatory contrast due to quantum interference of the Au(111) surface state[25]). In contrast, d*I*/d*V* maps recorded at sample biases that fall within the band gap exhibit no strong intensity on the ribbon. Figure 2C, for example, shows the 13-AGNR d*I*/d*V* map at a bias of 0.59 V, and the ribbon edges are dark. d*I*/d*V* mapping at biases corresponding to resonances either lower than the valence band edge or higher than the conduction band edge also reveal increased intensity near the GNR edges, but these maps additionally show stronger longitudinal nodal patterns than band edge d*I*/d*V* maps (see Supporting Information).

We also observe a midgap state localized near the short zigzag segment that marks the end of all nonreconstructed 13-AGNRs (which is the great majority of all observed nanoribbons). As seen in Figure 3A, the d*I*/d*V* spectrum recorded on the same 13-AGNR as shown in Figure 2 at a distance of 15 Å from such a zigzag end clearly reveals the presence of an "end state" at 0.20 ± 0.02 eV. The energies of the previously observed conduction and valence band edges remain unchanged. The end state feature is absent in "bulk" 13-AGNR spectra (*i.e.*, recorded at positions remote from the GNR terminus), as depicted in Figure 2A. We explored the spatial distribution of the end state by performing d*I*/d*V* mapping at a sample bias of 0.19 V on this nanoribbon. Figure 3C indicates that the end state is localized in close proximity to the short zigzag end of the 13-AGNR, extending only 30 Å along the GNR's longitudinal axis. Close-up STM images (Figures 3D and E, using a different 13-AGNR) reveal the precise position of all carbon atoms comprising the edges at

the end of a 13-AGNR (in Figure 3E a structural model of the 13-AGNR end region has been overlaid onto the STM image of Figure 3D).

The 13-AGNRs developed herein belong to the same subfamily of *n*-AGNRs ($n = 3p + 1$, with $p = 1, 2, 3, ...$) as 7-AGNRs, but have a band gap (1.4 eV) that is ~1.2 eV smaller than the one determined for 7-AGNRs.[19,20,24] This energy gap *vs* width trend is qualitatively consistent with theoretical models,[7,8,10] but the measured energy gaps are consistently narrower than those predicted by first-principles density functional theory (DFT) (2.4 eV for a 13-AGNR and 3.8 eV for a 7-AGNR, respectively).[10] This discrepancy likely arises from image charge screening due to the gold substrate, as has been shown for the $n = 7$ case.[20,26,27] Another inconsistency with theory is the fact that the experimental LDOS of the 13-AGNR conduction and valence band edge states are strongly localized along the edges of the ribbon (Figure 2B,D). This is in clear contrast to the spatially extended nature of the band edge states predicted for isolated AGNRs.[7,28] Similar spatial localization of band edge states has also been observed for 7-AGNRs on Au(111),[19,20] but no consistent explanation has been provided so far. The existence of stronger longitudinal nodal variation in the LDOS intensity along the 13-AGNR edges for resonances above (below) the conduction (valence) band edge suggests that these resonances are higher excited electron-like (hole-like) states of the GNRs, thus further supporting identification of the conduction (valence) band edge state (see Supporting Information). The experimentally observed 13-AGNR end state (Figure 3A,C) likely arises from the zigzag segment comprised of sp^2-hybridized carbon atoms localized at the ends of each 13-AGNR (Figure 3D,E). Related behavior has been observed at the ends of 7-AGNRs.[19]

The mechanism by which the linear growth of GNRs is truncated remains a crucial question. Comparison between Figures 3D and 3E indicates that, aside from the substitution of the terminal bromine atom by hydrogen, no further reconstruction of the edge atoms can be observed for 13-AGNRs. Since these nonreconstructed ends have no apparent bright spots associated with bromine atoms or apparent depressions induced by radical-surface interactions, 13-AGNRs are likely terminated by single hydrogen atoms (*i.e.*, one per carbon atom).[19,29] This is further supported by the observation of 13-AGNR localized end states (Figure 3A,C), which are associated with sp^2-hybridized C−H bonds. This leads us to deduce that two possible mechanisms for the truncation of 13-AGNR growth are (i) hydrogen abstraction during the chain-growth polymerization of the small-molecule precursor **1** at 200 °C and (ii) quenching of the aryl radical at the end of the chain during the 400 °C cyclization/dehydrogenation process. We are currently unable to distinguish between these two mechanisms.

CONCLUSIONS

We have demonstrated the atomically precise synthesis of 13-AGNRs on Au(111) *via* covalent self-assembly from small-molecule building blocks. We find that the energy gap of 13-AGNRs is 1.4 ± 0.1 eV, 1.2 eV narrower than the analogously defined band gap of a 7-AGNR. Spatially localized 13-AGNR end states are observed at 0.20 eV above the Fermi level in the region near zigzag ends. Our work demonstrates precise and controlled tunability of band gaps in bottom-up-fabricated semiconducting AGNRs through width variation. Such readily modifiable GNRs should help pave the way toward development of GNR-based semiconductor nanotechnology.

METHODS

A gold single crystal with polished Au(111) surface was used as the substrate for these experiments. Standard Ar^+ sputtering/annealing cycles were applied to obtain an atomically clean Au(111) surface. A home-built Knudsen cell was used to sublime the precursor molecule **1** at 206 °C. The deposition rate of the precursor molecule was 0.5 Å/min, as measured by a quartz crystal microbalance.

STM measurements were performed using a home-built STM with the samples held at 7 K in UHV. A PtIr tip was used for topography and spectroscopic measurements. Topography was obtained using the constant current mode of the STM. For d*I*/d*V* spectra the tunneling current was measured by a lock-in amplifier, while the sample bias was modulated by a 451 Hz, 5−10 mV (rms) sinusoidal voltage under open-feedback conditions. All STM images were processed by WSxM.[30]

Conflict of Interest: The authors declare no competing financial interest.

Supporting Information Available: General procedures, Scheme S1, synthesis of **1**, scanning tunneling spectroscopy of 7-AGNR, additional STM d*I*/d*V* spectra and d*I*/d*V* maps of 13-AGNR, and Figures S1−S4. This material is available free of charge *via* the Internet at http://pubs.acs.org.

Acknowledgment. Research was supported by the Office of Naval Research BRC Program (molecular synthesis and characterization), by the Helios Solar Energy Research Center, which is supported by the Director, Office of Science, Office of Basic Energy Sciences of the U.S. Department of Energy under Contract No. DE-AC02-05CH11231 (STM instrumentation development, STM operation), and by National Science Foundation award DMR-1206512 (image analysis). D.G.O. acknowledges fellowship support by the European Union under FP7-PEOPLE-2010-IOF.

REFERENCES AND NOTES

1. Fujita, M.; Wakabayashi, K.; Nakada, K.; Kusakabe, K. Peculiar Localized State at Zigzag Graphite Edge. *J. Phys. Soc. Jpn.* **1996**, *65*, 1920–1923.
2. Lee, H.; Son, Y.-W.; Park, N.; Han, S.; Yu, J. Magnetic Ordering at the Edges of Graphitic Fragments: Magnetic Tail Interactions between the Edge-Localized States. *Phys. Rev. B* **2005**, *72*, 174431.
3. Nakada, K.; Fujita, M.; Dresselhaus, G.; Dresselhaus, M. S. Edge State in Graphene Ribbons: Nanometer Size Effect and Edge Shape Dependence. *Phys. Rev. B* **1996**, *54*, 17954.

4. Pan, M.; Girão, E. C.; Jia, X.; Bhaviripudi, S.; Li, Q.; Kong, J.; Meunier, V.; Dresselhaus, M. S. Topographic and Spectroscopic Characterization of Electronic Edge States in CVD Grown Graphene Nanoribbons. *Nano Lett.* **2012**, *12*, 1928–1933.
5. Son, Y.-W.; Cohen, M. L.; Louie, S. G. Half-Metallic Graphene Nanoribbons. *Nature* **2007**, *446*, 342–342.
6. Tao, C.; Jiao, L.; Yazyev, O. V.; Chen, Y.-C.; Feng, J.; Zhang, X.; Capaz, R. B.; Tour, J. M.; Zettl, A.; Louie, S. G.; *et al*. Spatially Resolving Edge States of Chiral Graphene Nanoribbons. *Nat. Phys.* **2011**, *7*, 616–620.
7. Ezawa, M. Peculiar Width Dependence of the Electronic Properties of Carbon Nanoribbons. *Phys. Rev. B* **2006**, *73*.
8. Son, Y.-W.; Cohen, M. L.; Louie, S. G. Energy Gaps in Graphene Nanoribbons. *Phys. Rev. Lett.* **2006**, *97*, 216803.
9. Wassmann, T.; Seitsonen, A. P.; Saitta, A. M.; Lazzeri, M.; Mauri, F. Clar's Theory, π-Electron Distribution, and Geometry of Graphene Nanoribbons. *J. Am. Chem. Soc.* **2010**, *132*, 3440–3451.
10. Yang, L.; Park, C.-H.; Son, Y.-W.; Cohen, M. L.; Louie, S. G. Quasiparticle Energies and Band Gaps in Graphene Nanoribbons. *Phys. Rev. Lett.* **2007**, *99*, 186801.
11. Han, M.; Özyilmaz, B.; Zhang, Y.; Kim, P. Energy Band-Gap Engineering of Graphene Nanoribbons. *Phys. Rev. Lett.* **2007**, 98.
12. Hicks, J.; Shepperd, K.; Wang, F.; Conrad, E. H. The Structure of Graphene Grown on the SiC (000$\bar{1}$) Surface. *J. Phys. D: Appl. Phys.* **2012**, *45*, 154002.
13. Jiao, L.; Wang, X.; Diankov, G.; Wang, H.; Dai, H. Facile Synthesis of High-quality Graphene Nanoribbons. *Nat. Nanotechnol.* **2010**, *5*, 321–325.
14. Kang, C. G.; Kang, J. W.; Lee, S. K.; Lee, S. Y.; Cho, C. H.; Hwang, H. J.; Lee, Y. G.; Heo, J.; Chung, H.-J.; Yang, H.; *et al*. Characteristics of CVD Graphene Nanoribbon Formed by a ZnO Nanowire Hardmask. *Nanotechnology* **2011**, *22*, 295201.
15. Kato, T.; Hatakeyama, R. Site- and Alignment-Controlled Growth of Graphene Nanoribbons from Nickel Nanobars. *Nat. Nanotechnol.* **2012**, *7*, 651–656.
16. Kosynkin, D. V.; Higginbotham, A. L.; Sinitskii, A.; Lomeda, J. R.; Dimiev, A.; Price, B. K.; Tour, J. M. Longitudinal Unzipping of Carbon Nanotubes to Form Graphene Nanoribbons. *Nature* **2009**, *458*, 872–876.
17. Sprinkle, M.; Ruan, M.; Hu, Y.; Hankinson, J.; Rubio-Roy, M.; Zhang, B.; Wu, X.; Berger, C.; de Heer, W. A. Scalable Templated Growth of Graphene Nanoribbons on SiC. *Nat. Nanotechnol.* **2010**, *5*, 727–731.
18. Cai, J.; Ruffieux, P.; Jaafar, R.; Bier, M.; Braun, T.; Blankenburg, S.; Muoth, M.; Seitsonen, A. P.; Saleh, M.; Feng, X.; *et al*. Atomically Precise Bottom-up Fabrication of Graphene Nanoribbons. *Nature* **2010**, *466*, 470–473.
19. Koch, M.; Ample, F.; Joachim, C.; Grill, L. Voltage-Dependent Conductance of a Single Graphene Nanoribbon. *Nat. Nanotechnol.* **2012**, *7*, 713–717.
20. Ruffieux, P.; Cai, J.; Plumb, N. C.; Patthey, L.; Prezzi, D.; Ferretti, A.; Molinari, E.; Feng, X.; Müllen, K.; Pignedoli, C. A.; *et al*. Electronic Structure of Atomically Precise Graphene Nanoribbons. *ACS Nano* **2012**, *6*, 6930–6935.
21. Huang, H.; Wei, D.; Sun, J.; Wong, S. L.; Feng, Y. P.; Neto, A. H. C.; Wee, A. T. S. Spatially Resolved Electronic Structures of Atomically Precise Armchair Graphene Nanoribbons. *Sci. Rep.* **2012**, *2*, 983.
22. Weiler-Feilchenfeld, H.; Bergmann, E. D.; Hirschfeld, A. The Conformation of 9,9′-Bianthryl. *Tetrahedron Lett.* **1965**, *6*, 4129–4131.
23. Franc, G.; Gourdon, A. Covalent Networks through On-Surface Chemistry in Ultra-High Vacuum: State-of-the-Art and Recent Developments. *Phys. Chem. Chem. Phys.* **2011**, *13*, 14283–14292.
24. Linden, S.; Zhong, D.; Timmer, A.; Aghdassi, N.; Franke, J. H.; Zhang, H.; Feng, X.; Müllen, K.; Fuchs, H.; Chi, L.; *et al*. Electronic Structure of Spatially Aligned Graphene Nanoribbons on Au(788). *Phys. Rev. Lett.* **2012**, *108*, 216801.
25. Crommie, M. F.; Lutz, C. P.; Eigler, D. M. Imaging Standing Waves in a Two-Dimensional Electron Gas. *Nature* **1993**, *363*, 524–527.
26. Neaton, J. B.; Hybertsen, M. S.; Louie, S. G. Renormalization of Molecular Electronic Levels at Metal-Molecule Interfaces. *Phys. Rev. Lett.* **2006**, *97*, 216405.
27. Thygesen, K. S.; Rubio, A. Renormalization of Molecular Quasiparticle Levels at Metal-Molecule Interfaces: Trends across Binding Regimes. *Phys. Rev. Lett.* **2009**, *102*, 046802.
28. Hod, O.; Peralta, J.; Scuseria, G. Edge Effects in Finite Elongated Graphene Nanoribbons. *Phys. Rev. B* **2007**, *76*.
29. Talirz, L.; Söde, H.; Cai, J.; Ruffieux, P.; Blankenburg, S.; Jafaar, R.; Berger, R.; Feng, X.; Müllen, K.; Passerone, D.; *et al*. Termini of Bottom-Up Fabricated Graphene Nanoribbons. *J. Am. Chem. Soc.* **2013**, *135*, 2060–2063.
30. Horcas, I.; Fernández, R.; Gómez-Rodríguez, J. M.; Colchero, J.; Gómez-Herrero, J.; Baro, A. M. WSXM: A Software for Scanning Probe Microscopy and a Tool for Nanotechnology. *Rev. Sci. Instrum.* **2007**, *78*, 013705.